Journal of Physics and Chemistry of Solids 173 (2023) 111106

Contents lists available at ScienceDirect

Journal of Physics and Chemistry of Solids

journal homepage: www.elsevier.com/locate/jpcs

A noble metal-free candle soot derived carbon electrocatalyst for simultaneous H_2 generation and wastewater treatment

Swapna Pahra [a,b], Omkar Sangabathula [c], Chandra S. Sharma [c,**], Pooja Devi [a,*]

[a] Materials Science and Sensor Application, CSIR-Central Scientific Instruments Organisation, Chandigarh, 160030, India
[b] Academy of Scientific and Innovative Research, Ghaziabad, 201002, India
[c] Creative & Advanced Research Based on Nanomaterials (CARBON) Laboratory, Department of Chemical Engineering, Indian Institute of Technology Hyderabad, Kandi, Telangana, 502285, India

ARTICLE INFO

Keywords:
Water treatment
Carbon soot derived carbon
Hydrogen evolution reaction
Electrocatalyst
Waste water treatment

ABSTRACT

Electrocatalytic water splitting to produce green hydrogen is a promising approach for clean energy generation. However, the commercial aspect of this approach is limited due to catalysts cost and feedstock. Thus design of an inexpensive and noble metal-free (Pt, Rh, Ir etc.) catalyst is desirable. Moreover, wastewater as a feedstock for hydrogen generation is not explored to its full potential for green hydrogen generation, which otherwise is also a problem to be managed especially in developing countries. In the present work, we have investigated an inexpensive catalyst i.e. candle soot-derived carbon as an electrocatalyst for H_2 generation from textile wastewater utilizing methylene blue as a model pollutant. The carbon catalyst is synthesized from the candle soot and is characterized for its structural and morphological properties. Carbon soot coated onto the nickel foam (CS@NF) proves as an efficient hydrogen evolution catalyst due to its excellent electrical conductivity and large active surface area. $CS_{2.5}$@NF (with the loading of 2.5 mg cm^{-2}) shows an overpotential and Tafel slope of 117 mV and 43.85 mV/dec, respectively in an acidic medium containing textile pollutants. Under optimal condition, ~62% degradation is achieved within ~90 min, along with the stable hydrogen production of ~0.158 mmol per hour. These preliminary findings demonstrate the potential usage of an inexpensive non-noble metal free catalyst for simultaneous wastewater treatment as well as hydrogen generation.

1. Introduction

With increasing global environmental concerns and depleting fossil fuels due to high energy demand, it is high time to develop alternative sources of energy [1,2] Lately, green approach of energy generation have become more significant to meet the global energy demand, wherein, in recent times, hydrogen has become the perfect candidate for clean and green energy [3,4]. In 2014, the global market for molecular hydrogen (H_2) as a clean and high-density energy carrier as well as a chemical reagent for ammonia synthesis and petroleum and metals refining was anticipated to be worth more than 100 billion US dollars [5]. But the predominant (96%) production pathway for H_2 relies on fossil fuel transformation, such as steam reformation of methane, coal gasification, etc., due to their cost effectiveness. However, the carbon footprint of these technologies has a substantial environmental implications [6]. Alternatively, hydrogen production via electrochemical water splitting (EWS) using electricity as well as solar energy has evoked tremendous interest due to their advantages of zero carbon foot print, scalability and overall clean process [1,2].

Additionally, another major problem faced globally, especially, in developing countries is management of wastewater. With increase in urbanization and industrialization, groundwater and other fresh water bodies are getting contaminated due to unregulated release of untreated or partially treated wastewater. Industries, agricultural, and residential are the three major sectors responsible for the emission of pollutants into water bodies. Some of the most common organic pollutants are mostly industrial waste; pharmaceutical waste products, heavy metals, pesticides including insecticides, polynuclear hydrocarbons, halogenated aromatic compounds, microbes including bacteria, fungi, algae, virus and other worms, phenolic compounds, nitro or nitro-aromatic compounds and coloured dyes [7]. The textile industry, as well as its wastewater, has grown in response to rising demand for textile products.

* Corresponding author.
** Corresponding author.
E-mail addresses: cssharma@che.iith.ac.in (C.S. Sharma), poojaiitr@csio.res.in (P. Devi).

https://doi.org/10.1016/j.jpcs.2022.111106
Received 10 August 2022; Received in revised form 22 October 2022; Accepted 3 November 2022
Available online 12 November 2022

High pH, colour, nutrients (nitrogen and phosphorus), inorganic salts, and refractory organics are the most common contaminants found in textile effluent [8,9]. In general, it's treated by standard waste treatment techniques of adsorption, flocculation, advanced oxidation processes (biological, photochemical, ozonation, Fenton reaction), etc. However, these techniques have several disadvantages such as adsorption of dye on treating material, non-selectivity, formation of by-product in case of ozonation, requirement of inert environment in case of biological methods, requirement of low pH in case of Fenton reaction, etc., which in turn also leads to partial degradation of several organic constituents [10].

In light of above facts, a multifunctional catalyst that can simultaneously produce hydrogen via electrocatalysis and decontaminate the pollutant could be a great solution to the above problems. Noble metal-encompassing electrocatalysts (Pt, Rh, Ru, Ir, etc.) are currently considered cutting-edge state of art electrocatalysts, wherein platinum (Pt) and iridium dioxide (IrO_2) are generally employed for hydrogen evolution reaction (HER) and oxygen evolution reaction (OER), respectively, due to their high activity and fast kinetics [4]. However, they are expensive and rarely available earth elements, therefore their application at industrial level is limited [1,2,4]. Alternatively, other non-noble metal catalyst such as transition metal oxides [11,12],selenides [13,14], nitrides [15,16], borides [17], and phosphides [18] for HER, and transition metal oxides [19], hydroxides [20], and phosphates [21] for OER have shown promising results [4]. Despite of these remarkable reported works in this field there are still some gaps that have to be filled to replace the existing benchmarked catalysts especially in terms of cost and supply chain.

Recently, carbon materials have found tremendous applications in electrochemical energy harvesting and storage devices due to their advert advantages including high specific surface area, comparative chemical inertness, outstanding electronic conductivity and hierarchical pore size distribution [22–25]. But most of the research in these domains utilizes graphite, graphene, reduced graphene oxide (rGO), carbon nanotubes (CNT), etc., as carbon material due to their excellent properties listed above [26–31]. These materials have been used as conductive support in electrocatalytic water splitting as hybrid catalysts with transition metals mainly Ni, Co, Fe and their dichalcogenides. Few reported catalysts include Ni/rGO, Ni/Fe hydroxide nanoplates onto CNTs, Ni/NiO, Co–CoO on N-doped rGO, metal carbides M_3C/graphene nanoribbons [22]. Few metal-free carbon nanomaterials have also been investigated like CNTs, graphene sheets, graphite nanoplatelets, 3-D carbon structures in the field of catalysis for water splitting. Metal-free carbon nanomaterials are mainly nitrogen, boron or oxygen mono/-dual/tridoped which act as promising active catalysts for water splitting and their performance can be further improved by codoping with other heteroatoms (e.g. S or P) [22,32]. Despite huge progress in area of metal-free carbon based electrocatalysts, their application other than in ORR is yet a challenge [22]. Also some graphene/carbon blend-based electrocatalyst like CoS_2/RGO-CNT, Co@NCNTs@rGO, Mo_2C/G-NCS have been reported as HER electrocatalyst but their complicated synthesis processes sometimes leads to irreproducibility in their high performance [32]. Lyu et al. have also reported the graphene encapsulated Fe_3C nanoparticles coated onto stainless steel with an overpotential achieved was 264 mV at 10 $mAcm^{-2}$ for HER and 290 mV for 10 $mAcm^{-2}$ [33]. Some 3-D graphene based electrocatalysts have also been reported. Since the first theoretical transition metal phosphide for HER is reported in 2005 [34], Many electrocatalysts have been explored with their graphene based hybrids. Few 3-D graphene phosphides are CoP@C-NPs/GA [35], FeP/3DG20 [36], NiFeP/SG [37]. Transition metal chalcogenide has received a lot of interest in HER due to its distinct physicochemical property, good catalytic activity, and affordable cost compared to noble metals. Since MoS_2 has proven to be an excellent electrocatalyst for HER, researches have designed and reported its hybrid with various carbon material like 3D MoS_2/Graphene hierarchical hydrogel, 3D graphene supported MoSx NPs (MoSx/3D-graphene), 3D MoS_2–NiS_2/NGF. Many other materials have been integrated with 3D graphene which act a self-supported catalusts like Ni_2P-G/NF,3D Ni_3FeN NPs/r-GO aerogel, EG/$Co_{0.85}Se$/NiFe–LDH [38] but their synthesis methods are complicated and costly which make them inefficient candidates in the field of large scale production.

Graphene based nanoadsorbants have been widely reported for the removal of organic and inorganic contaminants in water/wastewater. They are mainly graphene based nanocomposites of transition metals/transition metal oxides such as Gs-Fe_3O_4, GOs-Fe_3O_4, GOs-Fe-Mn, rGOs-metal-Fe_2O_4, rGOs-Ni-Cr-CO_3, GOs-Fe-Mn, Gs-Ti nanotubes or graphene oxides based sponge/hydrogel/CNTs targeting contaminants like methylmercury, methylene blue, rhodamine B, crystal violet, methyl violet, tetracycline antibiotics, bisphenol A [39].

Even though having better properties, the synthesis procedure of these materials is time-consuming as well as requires corrosive chemicals and sophisticated laboratory equipment. Thus, there should be a simple way to mass-produce the carbon-based material, which is environmentally benign, cost-effective, and reusable for these kinds of applications. Carbon derived from candle soot generally contains spherical interconnected network of carbon particle that have sizes in the range of 20–50 nm and also exhibit high specific surface area [40,41]. The interconnected particles help in better electron transfer at electrode/electrolyte interface and high specific surface area helps in providing more catalytic sites, which in turn can results in achieving the better electrocatalytic properties [42,43]. However, it has not been widely investigated as an alternate carbon catalyst for electrocatalytic water splitting, especially wastewater, to the best of our knowledge.

In light of above research gaps, in the present work, we report for the first time, candle soot derived carbon nanoparticles network as an electrode material for electrocatalytic hydrogen generation from wastewater utilizing methylene blue (MB) as a model textile pollutant. MB is a heterocyclic dye with a wide range of industrial applications, however on its incomplete degradation, it accumulates in the environment and creates high toxicity, thus posing major environmental concerns [44]. The findings present in this work paves the way towards utility of this metal free catalysts for this category of application of simultaneous treatment as well as hydrogen generation from wastewater.

2. Experimental

2.1. Materials

All the chemicals were used as such without any further purification. MB dye and sulphuric acid (98%) were purchased from Loba Chemie Pvt. Ltd. to prepare synthetic wastewater. Distilled water used throughout the experiments was obtained from Millipore system. Candle was purchased from local market to collect the candle soot derived carbon. Nickel foam current collector was purchased from MTI Corporation, USA.

2.2. Synthesis of carbon catalyst electrode

Candle soot derived carbon was directly deposited on top of the nickel foam utilizing our established protocol, reported in previous work [40,45]. The wax candles were purchased from a local market in Sangareddy, Telangana, India and used as it is. A single step flame combustion process was used to synthesize the interconnected carbon nanoparticles of candle soot. Carbon soot was collected over a nickel foam substrate by placing it above the flame tip. To avoid any wax impurities, soot was collected from the entirely combusted outermost zone of the flame. Controlled loading of the candle soot on nickel foam was done by weighing measurements of nickel foam before and after catalyst coating for few seconds. The prepared carbon coated nickel foam was used as working electrode for further electrochemical studies.

2.3. Characterization studies

The surface morphology of the candle soot derived carbon was analyzed with Field Emission Scanning Electron Microscope (FESEM) (ZEISS ULTRA FEG55) and High-resolution Transmission electron microscopy (HRTEM) (JEOL JEM 2100). The crystal structure was characterized by X-ray diffraction (XRD) (PANalytical, Cu-Kα radiation with $\lambda = 1.5406$ Å). FTIR and Raman analyses were performed with Tensor 37 system (Bruker, USA) and WITec alpha 300 Raman system (532 nm laser), respectively. Further to determine the elemental and electronic states of elements present in the material, ESCA-Omicron X-ray photoelectron spectroscopy (XPS) analysis was done.

2.4. Electrochemical studies

All the electrochemical studies were carried out with an electrochemical workstation (Metrohm Autolab PGSTAT302N) in a conventional three-electrode system. An Ag/AgCl and platinum electrode were used as a reference and counter electrode, respectively. The electrolyte used was simulated wastewater (5 ppm MB dye in 0.5 M H_2SO_4). The as-prepared CS@NF was directly used as working electrode. Catalyst loading of 1 mg cm^{-2}, 2 mg cm^{-2} and 2.5 mg cm^{-2} on 1 × 1 cm^2 Nickel foam are named as CS_1@NF, CS_2@NF, $CS_{2.5}$@NF. The potential values were converted into RHE (reverse hydrogen electrode) according to the equation: E_{RHE} (V) = $E_{Ag/AgCl}$ (V) + 0.059 * pH + 0.197 (V). Linear sweep polarization curves were obtained by sweeping the potential from 0 to −1.25 V (vs. RHE) at a scan rate of 10 mV/s. Cyclic voltammetry was carried out in a potential window of −0.24 to −0.14 V at different scan rates for the Cdl calculation. Current-time-dependent studies were carried out for ~3 h for the optimal loaded catalyst.

3. Results and discussion

3.1. Characterization of candle soot derived carbon electrode

The surface functionalities of the synthesized carbon catalyst were analyzed with FT-IR and results are shown in Fig. 1 (a). The characteristic sharp peaks present at 1240 cm^{-1} and 1360 cm^{-1} are assigned to C–O functional group, whereas the peak at 1780 cm^{-1}, 1580 cm^{-1} and 3430 cm^{-1} correspond to C═O, C═C and –OH functional groups [40]. The presence of all functional groups confirms the purity of the carbon derived from candle soot [45]. Furthermore, the characteristic Raman spectrum of the carbon derived from candle soot (Fig. 1 (b)), shows the characteristic peaks at 1580 cm^{-1} and 1348 cm^{-1}, which are assigned as graphitic (G) and defect (D) band of the disordered carbon [43]. G band represents the E_{2g} phonon vibrations of sp^2 carbon, whereas D band represents the defective nature of the carbon. The I_D/I_G ratio of the material is calculated to be 1.09, which indicates the defective nature of the carbon than the graphitic nature, which could be beneficial for catalytic activity [45]. The morphological features of the as synthesized catalyst are further captured with FESEM (Fig. 1 (c)) and XRD (Fig. 1 (d)), which can be further compared with bare nickel foam (Fig. S1). From Fig. 1 (c), the interconnected spherical carbon particles network can be observed clearly. The high-magnification image (inset) reveals that the carbon derived candle soot has average particle size around 40–50 nm. XRD spectrum (Fig. 1 (d)), shows a hump around 2Θ of 25°, which corresponds to the (002) hkl plane of carbon and thus confirms the amorphous nature of the carbon derived from the candle soot. The peak at 43.5° corresponds to the weak crystalline (101) hkl plane [40]. From the XRD analysis, it is thus evident that the synthesized carbon catalyst contains both graphitic and amorphous carbon. The amorphous nature of the carbon helps in creating more electrochemical actives sites, which in turn can help in obtaining better electrochemical properties of the prepared electrode.

Fig. 2 displays the TEM images of candle soot derived carbon. It is evident from the figure that candle soot derived carbon particles are interconnected in nature which correlated with the FESEM image as presented above in Fig. 1. The high-resolution TEM image of CS in Fig. 2 (b, c) further shows that a single particle displayed an interconnected onion-like layered structure [46]. The onion ring-like morphology provides the larger active surface area to adsorb the water molecules and hence enhance the production of hydrogen [47]. Better electrons transfer can be achieved by the interconnected carbon particles and thus could help in the elevation of electrochemical nature of the electrode. Due to the small particle size, the diffusion path length will also be shorter and can results in increase in the contact between electrode/electrolyte interfaces [41].

Further to determine the chemical composition and bonding states of the samples, XPS analysis was performed (Fig. 3). A wide energy range XPS survey spectra, as shown in Fig. 3 (a), confirms the presence of

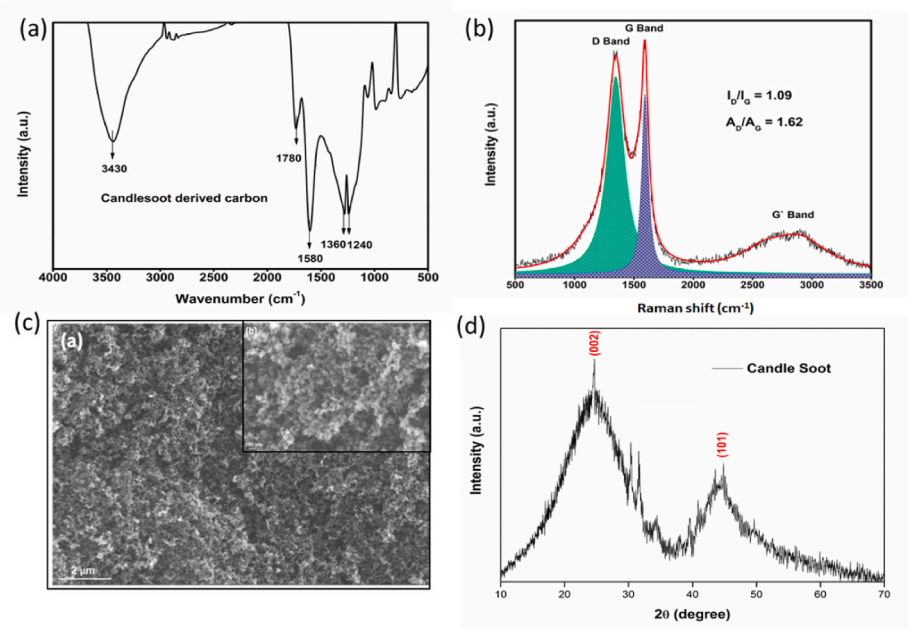

Fig. 1. (a) FT-IR (b) Raman (c) Low magnification and high magnification (inset) FE-SEM image and (d) XRD spectrum of carbon derived from candle soot.

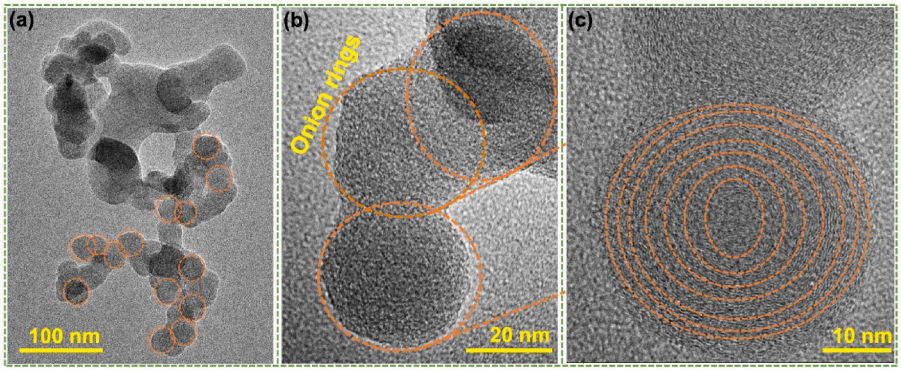

Fig. 2. (a) HR-TEM image of soot particles at (a) lower and (b), (c) higher magnification.

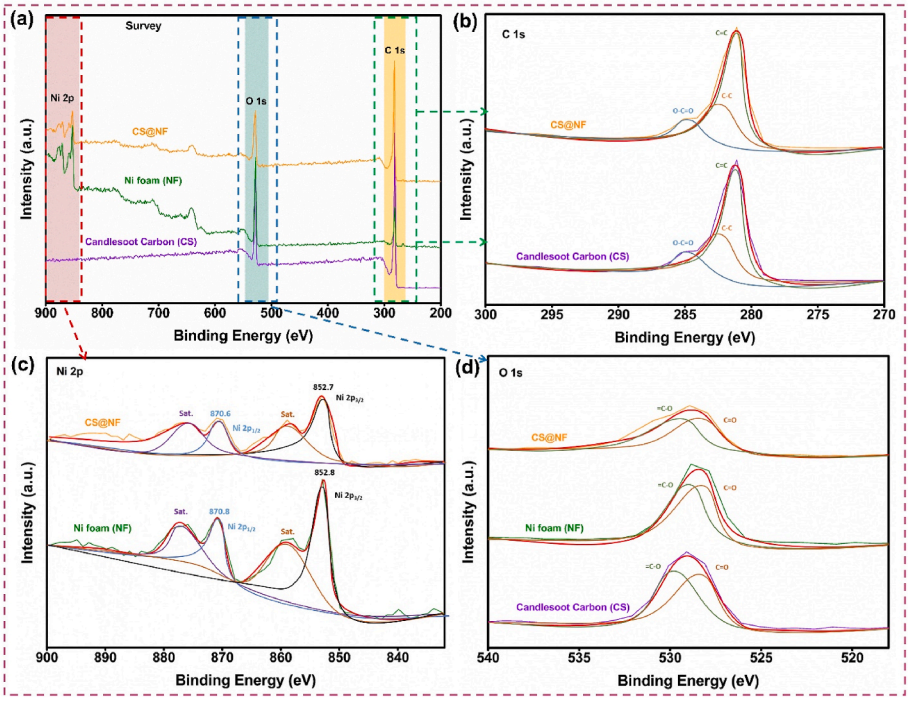

Fig. 3. (a) XPS survey scan and (b)–(d) core level C 1s, Ni 2p and O 1s spectra of candlesoot, bare NF and CS@NF, respectively.

Carbon (C), Oxygen (O) peaks from the Candle soot carbon sample (CS), whereas Ni foam (NF) and Candle soot coated Nickel foam (CS@NF) contains C, O and Ni elements. Fig. 3 (b) illustrates the de-convoluted spectra of C 1s, clearly confirming the chemical composition of CS and CS@NF [45]. The de-convoluted peak of CS consists of sp^3 hybridized carbon peaks (C–C, O–C═O) at 283.6, 285.1 eV, and sp^2 hybridized carbon peaks (C═C) at 282.4 eV, respectively. Similar peaks can also be observed in the CS@NF sample with a reduction in the intensity, and it's correlated with the existing literature [48,49]. The high-resolution de-convoluted Ni 2p spectra of NF and CS@NF are represented in Fig. 3 (c). Some traces of NiO is observed, which could be due to some partial oxidation of Ni electrodes. The peaks at the binding energies of 852.8 and 870.8 eV can be ascribed to the Ni $2p_{3/2}$ and Ni $2p_{1/2}$ of NiO of NF samples, whereas the peaks at 852.7 and 870.6 eV binding energies can be indicated as Ni $2p_{3/2}$ and Ni $2p_{1/2}$ of NiO. NiO enhance the charge transfer and hence electrical conductivity in the water splitting process [50–52]. The two satellite peaks of Nickel at 879.5 eV and 859.2 eV are related to the high binding energy side of Ni $2p_{3/2}$ and Ni $2p_{1/2}$ edge. It is worth noting that the Ni 2p spectra peak intensity for NF is significantly weaker than CS@NF because the coating of candle soot carbon on top of Ni foam reduced the intensity [53]. The de-convoluted Oxygen (1s) core spectrum (Fig. 3 (d)) comprises two peaks of C═O and = C–O at binding energies 528.1 and 531.6 eV, respectively [54]. The presence of adequate oxygen in carbon materials contributes to the electrode's wettability during electrochemical reactions and ultimately results in storing more charged ions at their surface. Furthermore, the electrode at the surface with a high degree of sp^2 hybridized carbon in CS@NF can maintain robust electrical conductivity [45,55,56].

3.2. Electro catalytic behavioural study of carbon catalyst

The electro catalytic behavioural study of the synthesized catalyst was done in 0.5 M H_2SO_4 containing 5 ppm MB as electrolyte. CS_n@NF electrode (1 × 1 cm^2) where n represents the loading of catalyst in mg cm^{-2}, were used as a working electrode. Linear sweep voltammetry (LSV) of electrodes with different catalyst loading amounts (1 mg cm^{-2}, 2 mg cm^{-2} and 2.5 mg cm^{-2}) is shown in Fig. 4. As it can be seen from the polarization curve (Fig. 4 (a)), $CS_{2.5}$@NF showed the highest current density of ~425 mA cm^{-2} at 1.25V (Vs. RHE) and an overpotential of 117 mV at 10 mA cm^{-2}, which is 245 mV for bare NF (ESI, Fig. S2). It

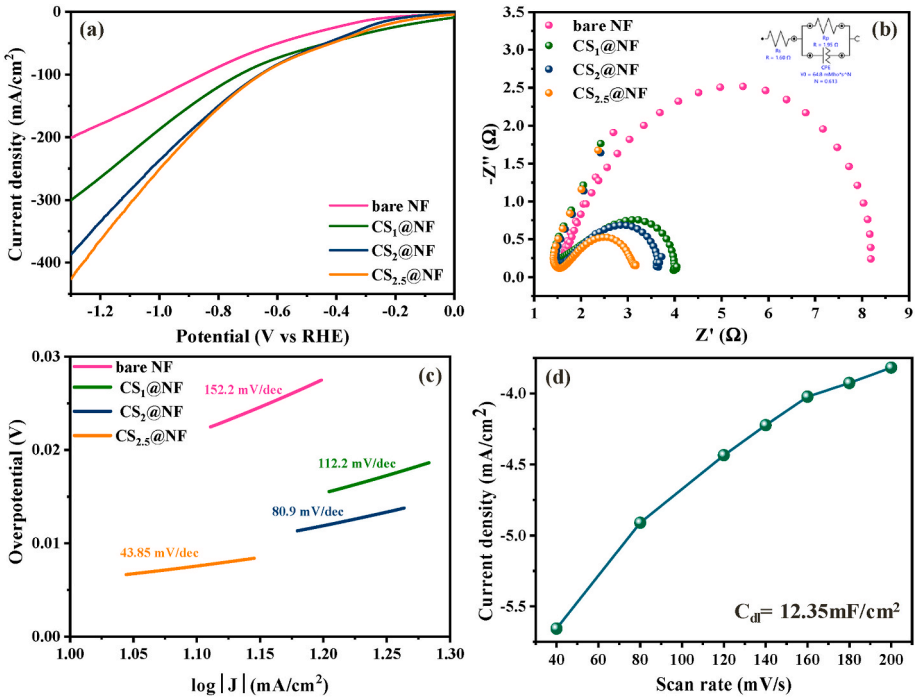

Fig. 4. (a) Polarization curve of CS_n@NF for HER at scan rate 10 mV/s (b) Nyquist plot (c) Tafel slope of CS_n@NF in 0.5 M H_2SO_4 containing 5 ppm MB and (d) electrochemical double-layer capacitance of $CS_{2.5}$@NF at 0.01Vvs RHE. (Inset: Randle's equivalent circuit for the CS_n@NF)

thus confirms that high loading of carbon catalyst enables high electrocatalytic activity and thus reduced overpotential. The charge transfer characteristics of the fabricated electrodes at electrode/electrolyte interface are further studied with EIS and results are shown in Fig. 4 (b). Particularly, charge transfer resistance (R_{ct}) obtained of catalyst was calculated as 6.661, 2.267, 1.868, 1.454 Ω for bare NF, CS_1@NF, CS_2@NF and $CS_{2.5}$@NF, respectively. Thus the results are in agreement with the polarization studies. Hence, $CS_{2.5}$@NF exhibited the excellent electro catalytic activity associated with the high loading of the carbon catalyst. Further loading of catalyst is observed in form of decrease in current density, which could be due to limited mass transfer.

The low overpotential obtained for the catalyst could be further understood by Tafel analysis. In general, HER in acidic media is dominated by two steps: the adsorption of hydrogen atoms onto the catalyst (known as Volmer step) and another is combination/desorption of hydrogen molecule from the catalyst surface (Heyrovsky or tafel step) as follows [2,57]:

$H_3O^+ + e^- \rightarrow H_{ads}$ (Volmer step reaction)

$H_{ads} + H_{ads} \rightarrow H_2$ (Heyrovsky)

$H^+ + H_{ads} + e^- \rightarrow H_2$ (Tafel step)

The Volmer, Heyrovsky and tafel steps are the rate determining steps (RDS). The cathodic current rises exponentially with the overpotential in all three processes but at different rates. Tafel slope thus helps to understand the mechanism at the catalyst surface and also understand the rate kinetics of the reaction for an electrocatalyst [58]. Therefore, Tafel slope of all the samples was calculated from LSV data and is shown in Fig. 2(c). CS_1@NF, CS_2@NF, $CS_{2.5}$@NF and bare nickel foam exhibit a Tafel slope of 112.2mV/dec, 80.9mV/dec, 43.85mV/dec and 152.2mV/dec, respectively. $CS_{2.5}$@NF showed the smallest Tafel slope value of 43.85mV/dec, which suggesting that the Heyrovsky step is the rate-determining step [57]. Further, to understand the effect of carbon soot loading on nickel foam, electrochemically active surface area (ECSA) was also calculated for the optimally performing catalyst loaded electrode by taking double-layer capacitance (C_{dl}) and specific capacitance (C_s) according to the formula: ECSA = C_{dl}/C_s [59]. C_{dl} was determined by taking cyclic voltammograms at different scan rate (20, 40, 80, 100, 120, 140, 160, 180, 200 mV/s) in a non-faradaic region (i.e. between −0.14 and −0.24 V vs. RHE (ESI, Fig. S4) and comes out to be 12.35 mF/cm^2 for $CS_{2.5}$@NF (Fig. 4(d)). Thus the corresponding ECSA was calculated to be 0.743 cm^2.

The above electrochemical characterizations thus reveal that amongst different carbon loaded catalyst, $CS_{2.5}$@NF outperformed. As in this study, MB was used as the model pollutant to study the degradation ability of CS_n@NF as well generation of hydrogen, thus its degradation was studied with all fabricated electrocatalysts i.e. CS_1@NF, CS_2@NF and $CS_{2.5}$@NF in chronoamperometry study. For this study, degradation experiments were performed at −117 mV (vs. RHE) for 90 min, and samples were collected at fixed intervals to study the degradation of MB with UV–Vis spectroscopy. MB exhibit a significant peak ~664 nm which corresponds to the n-π* transition in monomer molecules of the MB dye [60]. It can be seen from Fig. 5 (a) that the peak at 664 nm decreases with reaction time. At t_0 the absorbance was 0.38 a.u., which decreased to 0.141 a.u. for $CS_{2.5}$@NF (ESI, Fig. S2). Also, the degradation can be visibly witnessed through colorimetric change (Inset, Fig. 5 (a)). The colour of dye almost vanished after 90 min degradation study in case of $CS_{2.5}$@NF (inset, Fig. 5 (a)) as compared to bare Ni foam (inset, Fig. S3). Fig. 5 (b) shows the percent degradation comparison of $CS_{2.5}$@NF with bare Ni foam. Around 62% of dye degradation is achieved with $CS_{2.5}$@NF within 90 min which is higher than bare Ni foam and this behaviour can be assigned to high catalytic activity of coated carbon catalyst. While the bare Ni foam alone is not stable in acidic condition, thus the poor degradation activity is achieved for it. But the coating of the carbon catalysts enhanced its stability as well as activity [61]. The mechanism of dye degradation in this process could be understood in terms of generation of reactive oxygen species. In the current dual system, hydrogen is generated at cathode i.e. $CS_{2.5}$@NF, while dye is oxidized at anode. In general, OER is a competitive process to dye oxidation at anode. In general, OER is a complicated four electron process as it consists of formation of several intermediates such as O*, OH* and HOO*. MB dye is degrading at anode with intermediate OH* through ring opening mechanism with CO_2 and H_2O as the end products

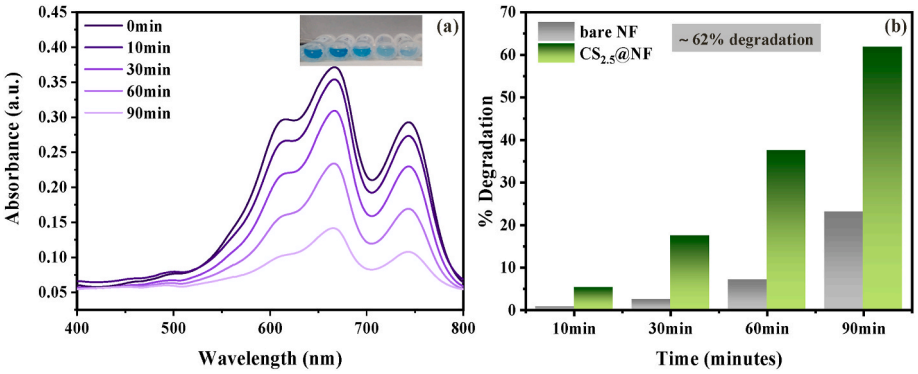

Fig. 5. (a) UV–Vis spectra of dye with $CS_{2.5}$@NF at different time intervals (inset: Naked eye colorimetric change in dye with time) and (b) Percent degradation of dye with $CS_{2.5}$@NF and bare NF.

[10]. On the other hand, talking about HER; the feasibility of OH* production at the cathode has recently been examined, albeit data is currently scarce. Some cathodes have the ability to create oxidizers like carbonaceous materials have been evaluated for H_2O_2 electro generation; possessing tremendous performance. It can be proposed that OH radical is generated through the reduction of O_2 to H_2O_2 at cathode. OH* destroys most organic pollutants mainly primarily through hydrogen abstraction or electrophilic addition to π systems that are present in organic pollutants [62]. Thus, generation of OH* at both anode and cathode could be responsible in achieving the degradation of MB dye during electrocatalysis.

To further study the kinetics of the degradation, the rate constant is determined from the relation between the concentration of the reactants and the reaction time. A linear relation between the change in concentration of the reactant (MB dye) and degradation time can be clearly seen from Fig. 6 (a) and (b). Therefore, it can be concluded from that the degradation of MB dye is following the pseudo first-order kinetics according to equation (1) [63].

$$\ln [C] = \ln[C_0] - kt \text{ or}$$

$$\ln [C]/[C_0] = -kt \quad (1)$$

Where, C and C_0 are the concentration of a reactant at time t and at time zero, respectively, k is rate constant and t is the time of the reaction. Rate constant, k, is calculated form the slope of the graph and found to be 0.16 min^{-1} and 0.63 min^{-1} for bare NF and $CS_{2.5}$@NF, respectively. Thus it can be concluded that the reaction rate is faster in case of $CS_{2.5}$@NF. The half-life of the reaction was also calculated and found to be 66s for MB dye degradation with $CS_{2.5}$@NF according to the formula: $t_{1/2} = \frac{\ln 2}{K}$, Where K is rate constant [63].

Another important factor that is of high importance for any electrocatalyst is its stability under wastewater environment. Hence, stability of the as prepared electrode $CS_{2.5}$@NF was checked at static overpotential −117mV (vs. RHE) in synthetic dye solution. It is observed that the current density almost remains the same for approximately 3 h (Fig. 7 (a)). Furthermore, the LSV of the electrocatalyst before and after stability studies remained unchanged, which confirms the stability of the $CS_{2.5}$@NF (Fig. 7(b)). The hydrogen production rate during chronoamperometric study is also calculated theoretically utilizing faradaic efficiency equation. The number of moles of hydrogen produced was calculated as 0.158 mmol per hour (calculated from equation (2)). Another factor to measure the catalytic activity is turnover frequency (TOF). TOF is a measure of a catalyst's instantaneous efficiency, measured as the derivative of the number of turnovers of the catalytic cycle [64]. Accordingly, TOF of the catalyst was also determined to be 5.7 X 10^{-6} s^{-1}.

$$No.\ of\ H_2\ moles\ produced = \frac{Faradaic\ Efficiency\ X\ current\ X\ time}{2F} \quad (2)$$

The performance of studied metal free electrocatalyst is also made with the previously reported work and is shown in Table 1. As can be seen, very limited efforts have been made on developing electrocatalyst especially HER catalyst for the simultaneous treatment as well as hydrogen generation from wastewater. Also, the reported catalysts are mainly based upon transition metals and further very little efforts have been made to use textile water as feedstock for hydrogen generation while also degrades the dye in process. The present work thus paves path of developing and utilizing inexpensive electrocatalyst based upon carbon for this domain. There is however further scope of improvements to increase the hydrogen production rate as well as the stability of the catalysis by tuning carbon morphology, crystallinity, defects, coating process, etc.

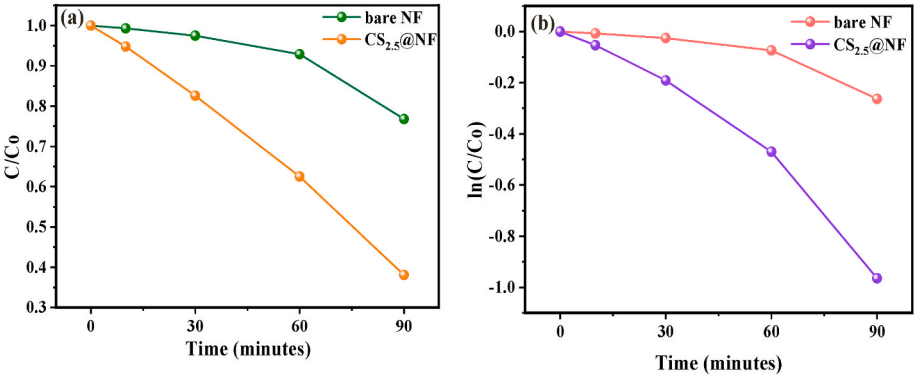

Fig. 6. Degradation performance of with bare NF and $CS_{2.5}$@NF (a) C/C_0 vs t, and (b) $\ln(C_0/C)$ vs for MB dye degradation in 0.5 M H_2SO_4.

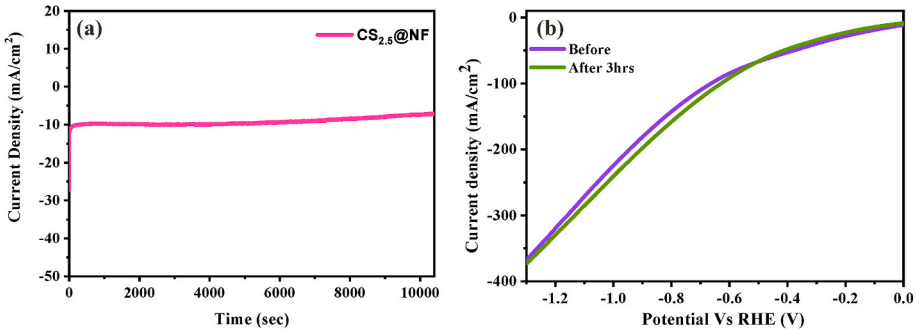

Fig. 7. (a) The chronoamperometric curve of $CS_{2.5}$@NF under static potential (−117 mV vs. RHE) and (b) The LSV curve of the catalyst before and after 3 h time-dependent testing.

Table 1
Comparative performance of $CS_{2.5}$@NF with reported literature in terms of HER activity.

Catalyst	Type of waste water treated	Overpotential (mV) at 10 mV/cm^2	Tafel slope (mV/dec)	C_{dl} (mF cm^{-2})	H_2 produced	Ref.
Sn–Pt–Co/Graphite	sewage water	–	46.2	0.04	–	[4]
Co_xP/Co_3O_4	Hydrazine Waste Water	HzOR-106	–	59.33	–	[1]
MoSx	Acidic industrial wastewater	130	100	–	–	[65]
$Ni_2P/Ni_{0.96S}$/NF	Urea based wastewater	72	149	110.26	–	[3]
Cr–C hybrids	Heavy metal wastewater	123	90	–	38.46 mmol g^{-1} h^{-1}	[66]
$Ni_{1.6}Co_{0.4}P$/C@HCNs	Urea based wastewater	145 in 1 M KOH	52.3	–		[67]
S–NiP_2Mo_5	Phenol containing water	1380 at 100 mA/cm^2	46	39.1	0.9–4.2 mol L^{-1}h^{-1}	[68]
SnS/NF	Urea based wastewater	192	152	25	–	[69]
CS@NF	Simulated Methylene blue textile Waste water	117	43.85	12.3	0.158 mmol h^{-1}	(This work)

4. Conclusions

In summary, we have successfully synthesized an inexpensive carbon based catalyst derived from candle soot i.e. CS_n@NF and demonstrated it for electrocatalytic hydrogen generation as well as wastewater treatment, using methylene blue as a model textile pollutant. The increase in catalyst loading is observed to increase the current density and reduced overpotential (117 mV at 10 mA/cm^2). The optimized catalyst is found to produce 0.158 mmol of hydrogen/hour along with the ~62% degradation of the MB within 90 min. The carbon-based inexpensive catalyst is also found to be stable in a harsh acidic condition of simulated textile water. Hence, this work provides a solution to both the environmental issue and opens up research in utilizing organic catalyst as an alternate to inorganic electrocatalyst.

Credit author statement

Swapna Pahra: Performed the experiments and analysis of data, Writing original draft. Omkar Sangabathula: Material fabrication and characterization analysis. Chandra. S. Sharma: Supervision, editing. Pooja Devi: Design of experiment, Methodology, supervision, formal analysis, review, editing, resources.

Declaration of competing interest

The authors declare that they have no known competing financial interests or personal relationships that could have appeared to influence the work reported in this paper.

Data availability

Data will be made available on request.

Acknowledgements

Authors are thankful to Director, CSIO for his kind permission to carry out this work. Funding support under WEA/2020/000022 is also acknowledged. Intial feasibility studies carried out by Dr. Anupma Thakur are also acknowledged.

Appendix A. Supplementary data

Supplementary data to this article can be found online at https://doi.org/10.1016/j.jpcs.2022.111106.

References

[1] X. Xu, T. Wang, W. Lu, L. Dong, H. Zhang, X. Miao, CoxP@Co3O4 Nanocomposite on Cobalt Foam as Efficient Bifunctional Electrocatalysts for Hydrazine-Assisted Hydrogen Production, ACS Sustainable Chem. Eng. 9 (2021) 4688–4701, https://doi.org/10.1021/acssuschemeng.1c00705.
[2] C.F. Du, X. Sun, H. Yu, Q. Liang, K.N. Dinh, Y. Zheng, et al., Synergy of Nb doping and surface alloy enhanced on water-alkali electrocatalytic hydrogen generation performance in Ti-based MXene, Adv. Sci. 6 (2019) 1–7, https://doi.org/10.1002/advs.201900116.
[3] M. He, C. Feng, T. Liao, S. Hu, H. Wu, Z. Sun, Low-cost Ni2P/Ni0.96S heterostructured bifunctional electrocatalyst toward highly efficient overall urea-water electrolysis, ACS Appl. Mater. Interfaces 12 (2020) 2225–2233, https://doi.org/10.1021/acsami.9b14350.
[4] A. Kumar, J. Hong, Y. Yun, H. Jung, K.S. Lee, J.W. Han, et al., A stable and active three-dimensional carbon based trimetallic electrocatalyst for efficient overall wastewater splitting, Int. J. Hydrogen Energy 46 (2021) 30762–30779, https://doi.org/10.1016/j.ijhydene.2021.06.193.
[5] K. Cho, M.R. Hoffmann, Molecular hydrogen production from wastewater electrolysis cell with multi-junction BiOx/TiO2 anode and stainless steel cathode: current and energy efficiency, Appl. Catal. B Environ. 202 (2017) 671–682, https://doi.org/10.1016/j.apcatb.2016.09.067.
[6] K. Cho, M.R. Hoffmann, Molecular hydrogen production from wastewater electrolysis cell with multi-junction BiOx/TiO2 anode and stainless steel cathode: current and energy efficiency, Appl. Catal. B Environ. 202 (2017) 671–682, https://doi.org/10.1016/j.apcatb.2016.09.067.

[7] V.K. Gupta, I. Ali, T.A. Saleh, A. Nayak, S. Agarwal, Chemical treatment technologies for waste-water recycling - an overview, RSC Adv. 2 (2012) 6380–6388, https://doi.org/10.1039/c2ra20340e.

[8] K. Sarayu, S. Sandhya, Current technologies for biological treatment of textile wastewater-A review, Appl. Biochem. Biotechnol. 167 (2012) 645–661, https://doi.org/10.1007/s12010-012-9716-6.

[9] S. Karthikeyan, A. Titus, A. Gnanamani, A.B. Mandal, G. Sekaran, Treatment of textile wastewater by homogeneous and heterogeneous Fenton oxidation processes, Desalination 281 (2011) 438–445, https://doi.org/10.1016/j.desal.2011.08.019.

[10] X. Teng, J. Li, Z. Wang, Z. Wei, C. Chen, K. Du, et al., Performance and mechanism of methylene blue degradation by an electrochemical process, RSC Adv. 10 (2020) 24712–24720, https://doi.org/10.1039/d0ra03963b.

[11] M.S. Alom, F. Ramezanipour, Layered oxides SrLaFe1-xCoxO4-δ (x=0-1) as bifunctional electrocatalysts for water-splitting, ChemCatChem 13 (2021) 3510–3516, https://doi.org/10.1002/cctc.202100867.

[12] M.S. Alom, C.C.W. Kananke-Gamage, F. Ramezanipour, Perovskite oxides as electrocatalysts for hydrogen evolution reaction, ACS Omega 7 (2022) 7444–7451, https://doi.org/10.1021/acsomega.1c07203.

[13] C. Tang, N. Cheng, Z. Pu, W. Xing, X. Sun, NiSe nanowire film supported on nickel foam: an efficient and stable 3D bifunctional electrode for full water splitting, Angew. Chem., Int. Ed. 54 (2015) 9351–9355, https://doi.org/10.1002/anie.201503407.

[14] L. Wang, J. Geng, W. Wang, C. Yuan, L. Kuai, B. Geng, Facile synthesis of Fe/Ni bimetallic oxide solid-solution nanoparticles with superior electrocatalytic activity for oxygen evolution reaction, Nano Res. 8 (2015) 3815–3822, https://doi.org/10.1007/s12274-015-0881-0.

[15] B. Cao, G.M. Veith, J.C. Neuefeind, R.R. Adzic, P.G. Khalifah, Mixed close-packed cobalt molybdenum nitrides as non-noble metal electrocatalysts for the hydrogen evolution reaction, J. Am. Chem. Soc. 135 (2013) 19186–19192, https://doi.org/10.1021/ja4081056.

[16] Z. Zhao, J. Zhao, H. Wang, X. Li, L. Yang, Z. Zhao, et al., Porous flower-like nickel nitride as highly efficient bifunctional electrocatalysts for less energy-intensive hydrogen evolution and urea oxidation, Int. J. Hydrogen Energy 45 (2020) 14199–14207, https://doi.org/10.1016/j.ijhydene.2019.11.007.

[17] S. Gupta, N. Patel, A. Miotello, D.C. Kothari, Cobalt-boride: an efficient and robust electrocatalyst for hydrogen evolution reaction, J. Power Sources 279 (2015) 620–625, https://doi.org/10.1016/j.jpowsour.2015.01.009.

[18] Z. Pu, J. Zhao, I.S. Amiinu, W. Li, M. Wang, D. He, et al., A universal synthesis strategy for P-rich noble metal diphosphide-based electrocatalysts for the hydrogen evolution reaction, Energy Environ. Sci. 12 (2019) 952–957, https://doi.org/10.1039/c9ee00197b.

[19] C. Bocca, A. Barbucci, M. Delucchi, G. Cerisola, Nickel - cobalt oxide-coated electrodes: influence of the preparation technique on oxygen evolution reaction (OER) in an alkaline solution, Int. J. Hydrogen Energy 24 (1999) 21–26, https://doi.org/10.1016/S0360-3199(98)00012-3.

[20] H. Liang, F. Meng, M. Cabán-Acevedo, L. Li, A. Forticaux, L. Xiu, et al., Hydrothermal continuous flow synthesis and exfoliation of NiCo layered double hydroxide nanosheets for enhanced oxygen evolution catalysis, Nano Lett. 15 (2015) 1421–1427, https://doi.org/10.1021/nl504872s.

[21] S.A. Khalate, S.A. Kadam, Y.R. Ma, S.S. Pujari, U.M. Patil, Cobalt doped iron phosphate thin film: an effective catalyst for electrochemical water splitting, J. Alloys Compd. 885 (2021), 160914, https://doi.org/10.1016/j.jallcom.2021.160914.

[22] C. Hu, L. Dai, Carbon-based metal-free catalysts for electrocatalysis beyond the ORR, Angew. Chem., Int. Ed. 55 (2016) 11736–11758, https://doi.org/10.1002/anie.201509982.

[23] J. Zhang, Z. Xia, L. Dai, Carbon-based electrocatalysts for advanced energy conversion and storage, Sci. Adv. 1 (2015), https://doi.org/10.1126/sciadv.1500564.

[24] C. Hu, R. Paul, Q. Dai, L. Dai, Carbon-based metal-free electrocatalysts: from oxygen reduction to multifunctional electrocatalysis, Chem. Soc. Rev. 50 (2021) 11785–11843, https://doi.org/10.1039/D1CS00219H.

[25] J. Wang, H. Kong, J. Zhang, Y. Hao, Z. Shao, F. Ciucci, Carbon-based electrocatalysts for sustainable energy applications, Prog. Mater. Sci. 116 (2021), 100717, https://doi.org/10.1016/j.pmatsci.2020.100717.

[26] C.E. Banks, T.J. Davies, G.G. Wildgoose, R.G. Compton, Electrocatalysis at graphite and carbon nanotube modified electrodes: edge-plane sites and tube ends are the reactive sites, Chem. Commun. (2005) 829–841, https://doi.org/10.1039/b413177k.

[27] H. Begum, M.S. Ahmed, Y.B. Kim, Nitrogen-rich graphitic-carbon@graphene as a metal-free electrocatalyst for oxygen reduction reaction, Sci. Rep. 10 (2020) 1–10, https://doi.org/10.1038/s41598-020-68260-3.

[28] S. Lu, M. Chen, Y. Wang, R. Li, J. Lin, X. Zhang, Highly efficient MoS2/rGO electrocatalysts for triiodide reduction as Pt-free counter electrode for dye-sensitized solar cells, Sol. Energy 220 (2021) 788–795, https://doi.org/10.1016/j.solener.2021.03.086.

[29] K keyan Arjunan, R. Rajakumaran, S. Sakthinathan, S.-M. Chen, T.-W. Chiu, S. Vinothini, Efficient electrocatalyst for hydrogen evolution reaction based on N-rGO-MWCNT/CuAlO 2 nanocomposite in acidic media, ECS J. Solid State Sci. Technol. 10 (2021), 045011, https://doi.org/10.1149/2162-8777/abf8fe.

[30] C. Huang, B. Zhang, Y. Luo, D. Xiao, K. Tang, Q. Ruan, et al., A hybrid Co NPs@CNT nanocomposite as highly efficient electrocatalyst for oxygen evolution reaction, Appl. Surf. Sci. 507 (2020), 145155, https://doi.org/10.1016/j.apsusc.2019.145155.

[31] G.A. Tafete, G. Thothadri, M.K. Abera, A review on carbon nanotube-based composites for electrocatalyst applications, Fullerenes, Nanotub. Carbon Nanostruct. (2022) 1–9, https://doi.org/10.1080/1536383X.2022.2028278, 0.

[32] H. Huang, M. Yan, C. Yang, H. He, Q. Jiang, L. Yang, et al., Graphene nanoarchitectonics: recent advances in graphene-based electrocatalysts for hydrogen evolution reaction, Adv. Mater. 31 (2019) 1–34, https://doi.org/10.1002/adma.201903415.

[33] Y. Lyu, R. Wang, L. Tao, Y. Zou, H. Zhou, T. Liu, et al., In-situ evolution of active layers on commercial stainless steel for stable water splitting, Appl. Catal. B Environ. 248 (2019) 277–285, https://doi.org/10.1016/j.apcatb.2019.02.032.

[34] P. Liu, J.A. Rodriguez, Catalysts for hydrogen evolution from the [NiFe] hydrogenase to the Ni 2P(001) surface: the importance of ensemble effect, J. Am. Chem. Soc. 127 (2005) 14871–14878, https://doi.org/10.1021/ja0540019.

[35] W. Zhao, X. Lu, M. Selvaraj, W. Wei, Z. Jiang, N. Ullah, et al., MXP(M = Co/Ni) @carbon core-shell nanoparticles embedded in 3D cross-linked graphene aerogel derived from seaweed biomass for hydrogen evolution reaction, Nanoscale 10 (2018) 9698–9706, https://doi.org/10.1039/c8nr02852d.

[36] D. Wang, J. Lu, L. Luo, S. Jing, H.S. Abbo, S.J.J. Titinchi, et al., Enhanced hydrogen evolution activity over microwave-assisted functionalized 3D structured graphene anchoring FeP nanoparticles, Electrochim. Acta 317 (2019) 242–249, https://doi.org/10.1016/j.electacta.2019.05.153.

[37] R.Q. Li, B.L. Wang, T. Gao, R. Zhang, C. Xu, X. Jiang, et al., Monolithic electrode integrated of ultrathin NiFeP on 3D strutted graphene for bifunctionally efficient overall water splitting, Nano Energy 58 (2019) 870–876, https://doi.org/10.1016/j.nanoen.2019.02.024.

[38] P. Kuang, M. Sayed, J. Fan, B. Cheng, J. Yu, 3D graphene-based H2-production photocatalyst and electrocatalyst, Adv. Energy Mater. 10 (2020) 1–53, https://doi.org/10.1002/aenm.201903802.

[39] S. Kim, C.M. Park, M. Jang, A. Son, N. Her, M. Yu, et al., Aqueous removal of inorganic and organic contaminants by graphene-based nanoadsorbents: a review, Chemosphere 212 (2018) 1104–1124, https://doi.org/10.1016/j.chemosphere.2018.09.033.

[40] M. Kakunuri, C.S. Sharma, Candle soot derived fractal-like carbon nanoparticles network as high-rate lithium ion battery anode material, Electrochim. Acta 180 (2015) 353–359, https://doi.org/10.1016/j.electacta.2015.08.124.

[41] O. Sangabathula, D. Potphode, C.S. Sharma, Morphology-controlled molybdenum disulfide/candle soot carbon composite for high-performance supercapacitor, ChemistrySelect 5 (2020) 6809–6817, https://doi.org/10.1002/slct.202001443.

[42] P. Rani, K.K. Sarode, M. Gaikwad, A.D. Pathak, C.S. Sharma, Internment of polysulfide in fractal carbon structure for high rate lithium-sulfur batteries, Appl. Surf. Sci. 564 (2021), 150294, https://doi.org/10.1016/j.apsusc.2021.150294.

[43] A.D. Pathak, D. Potphode, C.S. Sharma, Graphitization induced structural transformation of candle soot carbon into carbon nano-onion as a functional anode for metal-ion batteries, Mater Adv 3 (2022) 3610–3619, https://doi.org/10.1039/d2ma00042c.

[44] H. Safardoust-Hojaghan, M. Salavati-Niasari, Degradation of methylene blue as a pollutant with N-doped graphene quantum dot/titanium dioxide nanocomposite, J. Clean. Prod. 148 (2017) 31–36, https://doi.org/10.1016/j.jclepro.2017.01.169.

[45] D. Potphode, C.S. Sharma, Pseudocapacitance induced candle soot derived carbon for high energy density electrochemical supercapacitors: non-aqueous approach, J. Energy Storage 27 (2020), 101114, https://doi.org/10.1016/j.est.2019.101114.

[46] C. Yang, Z. Li, Y. Huang, K. Wang, Y. Long, Z. Guo, et al., Continuous roll-to-roll production of carbon nanoparticles from candle soot, Nano Lett. 21 (2021) 3198–3204, https://doi.org/10.1021/acs.nanolett.1c00452.

[47] A.L. Sangle, S. Singh, J. Jian, S.R. Bajpe, H. Wang, N. Khare, et al., Very high surface area mesoporous thin films of SrTiO3 grown by pulsed laser deposition and application to efficient photoelectrochemical water splitting, Nano Lett. 16 (2016) 7338–7345, https://doi.org/10.1021/acs.nanolett.6b02487.

[48] A. Gopalakrishnan, C.S. Sharma, High-performance dual carbon Li-ion hybrid capacitor constructed from N, S - co-doped candle soot derived carbon nanoparticles anode and porous carbon cathode, J. Energy Storage 55 (2022), 105788, https://doi.org/10.1016/j.est.2022.105788.

[49] R. Kanakaraj, C. Sudakar, Candle soot carbon nanoparticles as high-performance universal anode for M-ion (M = Li+, Na+ and K+) batteries, J. Power Sources 458 (2020), 228064, https://doi.org/10.1016/j.jpowsour.2020.228064.

[50] Z. Zhang, S. Liu, F. Xiao, S. Wang, Facile synthesis of heterostructured nickel/nickel oxide wrapped carbon fiber: flexible bifunctional gas-evolving electrode for highly efficient overall water splitting, ACS Sustain. Chem. Eng. 5 (2017) 529–536, https://doi.org/10.1021/acssuschemeng.6b01879.

[51] K. Fominykh, J.M. Feckl, J. Sicklinger, M. Döblinger, S. Böcklein, J. Ziegler, et al., Ultrasmall dispersible crystalline nickel oxide nanoparticles as high-performance catalysts for electrochemical water splitting, Adv. Funct. Mater. 24 (2014) 3123–3129, https://doi.org/10.1002/adfm.201303600.

[52] J. Liang, Y.Z. Wang, C.C. Wang, S.Y. Lu, In situ formation of NiO on Ni foam prepared with a novel leaven dough method as an outstanding electrocatalyst for oxygen evolution reactions, J. Mater. Chem. 4 (2016) 9797–9806, https://doi.org/10.1039/c6ta03729a.

[53] X. Hu, X. Tian, Y.W. Lin, Z. Wang, Nickel foam and stainless steel mesh as electrocatalysts for hydrogen evolution reaction, oxygen evolution reaction and overall water splitting in alkaline media, RSC Adv. 9 (2019) 31563–31571, https://doi.org/10.1039/c9ra07258f.

[54] Y. Ren, Y. Yan, Y. Wang, H. Zhang, X. Li, Thermally treated candle soot as a novel catalyst for hydrogen peroxide in-situ production enhancement in the bio-electro-Fenton system, Chemosphere 262 (2021), 127839, https://doi.org/10.1016/j.chemosphere.2020.127839.

[55] K.B. Pu, J.Y. Gao, W.F. Cai, Q.Y. Chen, K. Guo, Y. Huang, et al., A new modification method of metal substrates via candle soot to prepare effective anodes in air-cathode microbial fuel cells, J. Chem. Technol. Biotechnol. 97 (2022) 189–198, https://doi.org/10.1002/jctb.6928.
[56] J. Wang, Y. Chen, Oil-water separation capability of superhydrophobic fabrics fabricated via combining polydopamine adhesion with lotus-leaf-like structure, J. Appl. Polym. Sci. 132 (2015) 1–6, https://doi.org/10.1002/app.42614.
[57] J. Theerthagiri, S.J. Lee, A.P. Murthy, J. Madhavan, M.Y. Choi, Fundamental aspects and recent advances in transition metal nitrides as electrocatalysts for hydrogen evolution reaction: a review, Curr. Opin. Solid State Mater. Sci. 24 (2020), 100805, https://doi.org/10.1016/j.cossms.2020.100805.
[58] J. Yu, G. Li, H. Liu, A. Wang, L. Yang, W. Zhou, et al., Simultaneous water recovery and hydrogen production by bifunctional electrocatalyst of nitrogen-doped carbon nanotubes protected cobalt nanoparticles, Int. J. Hydrogen Energy 43 (2018) 12110–12118, https://doi.org/10.1016/j.ijhydene.2018.04.210.
[59] P. Connor, J. Schuch, B. Kaiser, W. Jaegermann, The determination of electrochemical active surface area and specific capacity revisited for the system MnOx as an oxygen evolution catalyst, Z. Phys. Chem. 234 (2020) 979–994, https://doi.org/10.1515/zpch-2019-1514.
[60] A. Ghanadzadeh, A. Zeini, A. Kashef, M. Moghadam, Concentration effect on the absorption spectra of oxazine1 and methylene blue in aqueous and alcoholic solutions, J. Mol. Liq. 138 (2008) 100–106, https://doi.org/10.1016/j.molliq.2007.09.005.
[61] C. Ruan, P. Li, J. Xu, Y. Xie, Electrochemical performance of hybrid membrane of polyaniline layer/full carbon layer coating on nickel foam, Prog. Org. Coating 139 (2020), 105455, https://doi.org/10.1016/j.porgcoat.2019.105455.
[62] A. Medel, J. Treviño-Reséndez, E. Brillas, Y. Meas, I. Sirés, Contribution of cathodic hydroxyl radical generation to the enhancement of electro-oxidation process for water decontamination, Electrochim. Acta 331 (2020), 135382, https://doi.org/10.1016/j.electacta.2019.135382.
[63] M.A. Mahmoud, A. Poncheri, Y. Badr, M.G. Abd El Waned, Photocatalytic degradation of methyl red dye, South Afr. J. Sci. 105 (2009) 299–303, https://doi.org/10.4102/sajs.v105i7/8.86.
[64] S. Kozuch, J.M.L. Martin, “Turning over” definitions in catalytic cycles, ACS Catal. 2 (2012) 2787–2794, https://doi.org/10.1021/cs3005264.
[65] M. Kokko, F. Bayerköhler, J. Erben, R. Zengerle, P. Kurz, S. Kerzenmacher, Molybdenum sulphides on carbon supports as electrocatalysts for hydrogen evolution in acidic industrial wastewater, Appl. Energy 190 (2017) 1221–1233, https://doi.org/10.1016/j.apenergy.2016.12.097.
[66] Y. Zhou, W. Zhou, D. Hou, G. Li, J. Wan, C. Feng, et al., Metal-carbon hybrid electrocatalysts derived from ion-exchange resin containing heavy metals for efficient hydrogen evolution reaction, Small 12 (2016) 2768–2774, https://doi.org/10.1002/smll.201503100.
[67] S. Rezaee, S. Shahrokhian, 3D ternary Ni: XCo2- xP/C nanoflower/nanourchin arrays grown on HCNs: a highly efficient bi-functional electrocatalyst for boosting hydrogen production via the urea electro-oxidation reaction, Nanoscale 12 (2020) 16123–16135, https://doi.org/10.1039/d0nr04616g.
[68] Y. Zheng, X. Xu, Surface atom regulation on polyoxometalate electrocatalyst for simultaneous low-voltage H2Production and phenol degradation, ACS Appl. Mater. Interfaces 12 (2020) 53739–53748, https://doi.org/10.1021/acsami.0c14431.
[69] S.A. Patil, H.T. Bui, S. Hussain, I. Rabani, Y. Seo, J. Jung, et al., Self-standing SnS nanosheet array: a bifunctional binder-free thin film catalyst for electrochemical hydrogen generation and wastewater treatment, Dalton Trans. 50 (2021) 12723–12729, https://doi.org/10.1039/d1dt01855h.